ELSEVIER

Physica B 273–274 (1999) 453–457

PHYSICA B

www.elsevier.com/locate/physb

A combined experimental and theoretical approach to grain boundary structure and segregation

S.J. Pennycook[a,b,*], M.F. Chisholm[a], Y. Yan[c], G. Duscher[a,b], S.T. Pantelides[a,b]

[a]*Solid State Division, Oak Ridge National Laboratory, PO Box 2008, Oak Ridge, TN 37831-6030, USA*
[b]*Department of Physics and Astronomy, Vanderbilt University, Nashville TN 37235, USA*
[c]*National Renewable Energy Laboratory, Golden, CO 80401, USA*

Abstract

Recently, the scanning transmission electron microscope has become capable of forming electron probes of atomic dimensions. Through the technique of Z-contrast imaging, it is now possible to form atomic resolution images with high compositional sensitivity from which atomic column positions can be directly determined. An incoherent image of this nature also allows atomic resolution chemical analysis to be performed, by locating the probe over particular columns or planes seen in the image while electron energy loss spectra are collected. Such data represent either an ideal starting point for first-principles theoretical calculations or a test of theoretical predictions. We present several examples where theory and experiment together give a very complete and often surprising atomic scale view of complex materials. © 1999 Elsevier Science B.V. All rights reserved.

Keywords: Grain boundaries; Atomic structure; Impurities; Segregation; Transformation; Electron microscopy; Total energy calculations

1. Direct imaging with electrons

The images we see with our eyes generally appear to be a direct representation of the world around us. This is because they are formed *incoherently*; objects are illuminated by light over a large range of directions and the intensity scattered depends primarily on the nature of the object and not on the direction of illumination. If objects are illuminated by coherent laser light they show a speckle pattern, which is due to interference effects. These are directly related to the object, but not in a manner that can be directly interpreted. Except for special applications, optical instruments such as a projector or a microscope invariably use incoherent illumination to maintain this capability for direct interpretation.

It is over one hundred years since Lord Rayleigh first explained the difference between coherent and incoherent imaging in the context of the light microscope. He clearly pointed out the advantages of incoherent imaging: absence of interference artifacts, and in addition a factor of two improved resolution [1]. Ideally, a self-luminous object is required for perfect incoherent imaging, so that each point will emit light independently. But Lord Rayleigh showed how the condenser lens can be used to give a close approximation to incoherent imaging. If the condenser lens subtends a sufficiently large range of angles, then we approach the incoherent imaging conditions of normal vision. Specifically, for an illumination semiangle θ, the transverse coherence length in the sample, ℓ_T, is $0.61\lambda/\theta$, which can be made comparable to the resolution limit.

In the conventional transmission electron microscope (CTEM), historically, a small condenser aperture has been used to give an approximation to perfect coherent imaging. This is necessary for low-resolution diffraction contrast imaging of defects such as dislocations, but this

* Correspondence address. Solid State Division, Oak Ridge National Laboratory, P.O. Box 2008, Oak Ridge, TN 37831-6030, USA. Tel.: + 1-423-574-5504; fax: + 1-423-574-4143.
E-mail address: pky@ornl.gov (S.J. Pennycook)

0921-4526/99/$ - see front matter © 1999 Elsevier Science B.V. All rights reserved.
PII: S0921-4526(99)00521-9

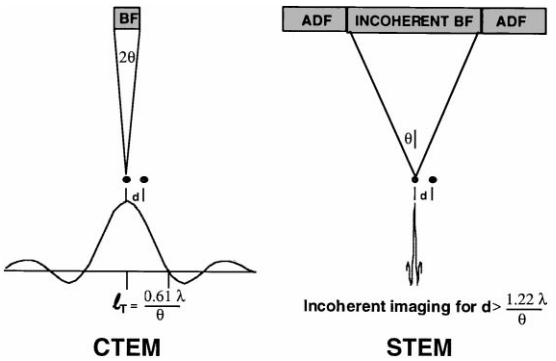

Fig. 1. Schematic comparing the transverse coherence lengths for coherent and incoherent imaging. In bright field (BF) conventional TEM the coherence length is large compared to interatomic spacings, whereas in the STEM, a large-angle BF or annular dark field (ADF) detector effectively breaks the coherence between neighboring atoms.

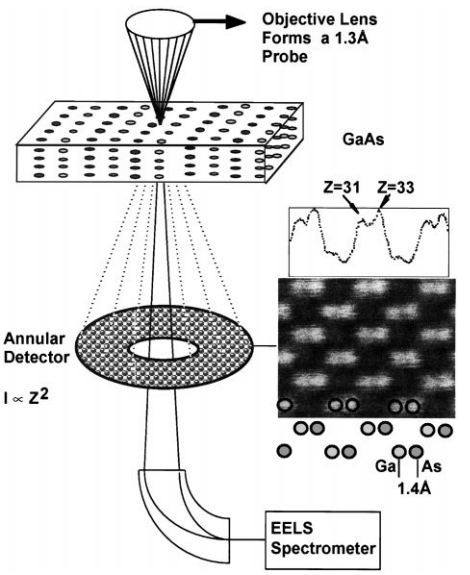

Fig. 2. Schematic showing a fine probe formed by the objective lens of an STEM. A Z-contrast image is formed by mapping high-angle scattered electrons as the probe is scanned across the sample, while atomic resolution electron energy loss spectroscopy is possible with the probe stationary on specific columns selected from the image. The Z-contrast image of GaAs shows As columns with higher intensity than Ga.

leads to a transverse coherence length much greater than typical interatomic spacings as shown in Fig. 1. As electron microscope resolution gradually improved it became possible to resolve atomic-scale features, but the coherent imaging conditions were maintained. In a coherent image (referred to as a phase contrast image) atomic columns can be bright or dark depending on specimen thickness and objective lens focus (which alter the relative phases of the scattered beams). It is clear that simply increasing the illumination aperture will reduce the transverse coherence length. Eventually, it will reduce below the typical interatomic spacings of materials, and the coherence between columns will be broken. We would then achieve incoherent imaging, and we would expect atomic images to become directly interpretable. This has indeed proved to be the case. In practice, however, it is more efficient and results in higher image contrast to reverse the direction of the electrons, and to use the complementary high-angle annular *detector* shown in Fig. 1. Then the image is formed by scanning the illumination across the sample, a scanning transmission electron microscope (STEM).

The principle of Z-contrast imaging in the STEM is shown schematically in Fig. 2. A small electron probe is scanned across a thin specimen, and the Z-contrast image results from mapping the intensity of electrons reaching the annular detector [2–7]. The detector performs the function of Lord Rayleigh's condenser lens. But it not only breaks the coherence in the *transverse* plane [8], it enforces high scattering angles, so that Rutherford scattering dominates and atoms contribute to the image with a brightness determined by their mean square atomic number Z. For this reason the image is referred to as a Z-contrast image. In a crystal, Rutherford scattering becomes phonon scattering, and effectively breaks the coherence through the *thickness* of the sample [9]. The thickness dependence of the image becomes relatively intuitive, and atomic images from thicker materials can be interpreted equally well on the basis of Z-contrast.

In the image of GaAs shown in Fig. 2, bright features correspond directly to columns of As, and the less bright features to columns of Ga. Unlike the coherent imaging of conventional high-resolution electron microscopy (HREM), the positions of atomic columns can be determined directly and uniquely from the image to a high accuracy, without the need for extensive image simulations of model structures. Incoherent imaging effectively bypasses the phase problem of HREM, a particular advantage for complex materials. The VG Microscopes HB603U STEM at ORNL has a 300 kV accelerating voltage, and a directly interpretable resolution of 1.26 Å, although recently information transfer at 0.78 Å has been demonstrated in Si⟨1 1 0⟩ [10]. This also demonstrates the factor of two improved resolution available with incoherent imaging; the comparable phase contrast image resolution on this microscope is 1.93 Å. There are now many examples where the high resolution and the direct interpretability of Z-contrast imaging have proved very successful. Examples include the direct determination of dislocation core structures in GaN [11] and at CdTe/GaAs interfaces [12], and in imaging structure and

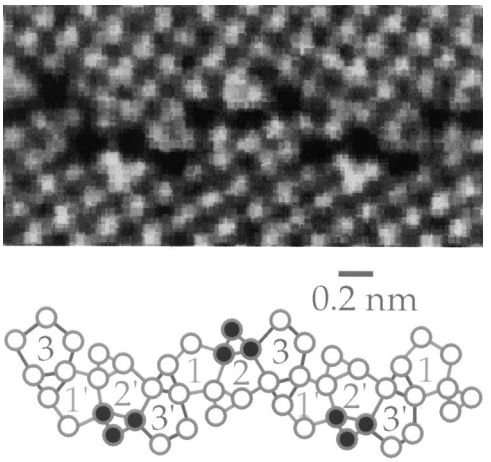

Fig. 3. Z-contrast image of a 23° ⟨0 0 1⟩ tilt grain boundary in Si showing its unexpectedly complex structure. The five-fold rings (with black centers in the image) are dislocation cores arranged in a repeating sequence along the boundary. Columns shown black in the schematic are those seen brighter in the image due to segregated As.

impurity sites at grain boundaries, as shown in the examples below.

The ability to retrieve atomic structures directly from experiment is a great advantage for first principles simulations, as it avoids the need to calculate large numbers of trial structures. This is especially true for complex materials where there are a great many possibilities. A further advantage of the STEM is that it allows electron energy loss spectroscopy (EELS) to be performed simultaneously with the Z-contrast image, allowing compositional analysis and local band structure to be determined at atomic resolution [13,14].

2. Arsenic segregation sites at a silicon grain boundary

Z-contrast imaging enables low concentrations of high-Z impurities to be directly observed. A recent example of this capability is shown in Fig. 3, a Z-contrast image from a 23° grain boundary in Si, after doping with As [15].

The atomic structure of the boundary is directly determined from the positions of the bright features in the image, and is different from all structures proposed previously. It comprises a continuous sequence of dislocation cores, a perfect edge dislocation (1) and two perfect mixed dislocations (2,3) arranged as a dipole, followed by the same sequence (1′,2′,3′) mirrored across the boundary plane. In the ⟨0 0 1⟩ projection, these dislocations appear as a connected array of pentagonal and triangular arrangements of atomic columns. The presence of the dipoles is surprising, as being of equal and opposite Burgers vector they could equally well be replaced by perfect crystal. However, precisely the same atomic arrangement is seen in the undoped boundary given the same annealing treatment.

Looking closely at the relative intensities of the columns in the doped sample, it is seen that one of the dislocation cores contains columns that are 20% brighter on average than other similar columns. This must be due to the presence of the As dopant. Taking into account the scattering cross section, the increased intensity corresponds to an average of only 5% As concentration, approximately two As atoms in each atomic column.

In a previous theoretical study of the shorter-period 36° grain boundary, it was found that isolated As atoms have only a small segregation energy of ~ 0.1 eV, too small to account for the concentrations observed experimentally [16]. However, as arsenic prefers to be three-fold coordinated, calculations were performed for arsenic dimers. It was found that the two As atoms repel and become three-fold coordinated without having to create an Si dangling bond. Thus binding of the dimer occurs through repulsion. After the image of Fig. 3 was obtained, calculations were repeated for the 23° boundary, and preference was found for those sites seen bright in the image. The segregation energy was again increased, becoming consistent with the As solubility limit in the bulk at the annealing temperature of 700°C. This combined use of experimental and theoretical techniques produced a remarkably detailed and consistent atomic-scale picture of impurity segregation at this grain boundary.

Very recently, an extensive ab initio study has confirmed the observed grain boundary structure, with its redundant dislocations, to be energetically preferred in the undoped grain boundary [17]. Further theoretical work could build on these results to determine grain boundary diffusion coefficients, as well as to extend studies to other boundaries and polycrystalline materials.

3. Impurity-induced grain boundary transformation in MgO

In Fig. 4, STEM imaging of an MgO grain boundary [18] reveals a structure that is inconsistent with the widely accepted structure of the boundary proposed by Harris et al. [19], based on theoretical modeling using classical potentials. The observed structure is similar to that proposed much earlier by Kingery [20]. The large empty core of the Harris structure is obviously very different from the more dense core of the Kingery model. On careful examination of the intensity in the experimental image, it can be seen that certain specific atomic columns at the grain boundary are again significantly brighter than neighboring columns, as arrowed in the figure. This suggests that impurities, with $Z > 12$, may be segregated at these sites. EELS measurements indeed

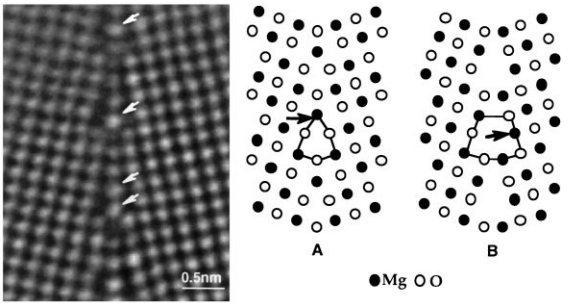

Fig. 4. Z-contrast image from a 24° ⟨0 0 1⟩ tilt grain boundary in MgO showing occasional bright atomic columns at the grain boundary (arrowed), compared to two structures for the 36° ⟨0 0 1⟩ tilt grain boundary proposed by (a) Kingery [20] and (b) Harris et al. [19]. Sites of Ca segregation are arrowed.

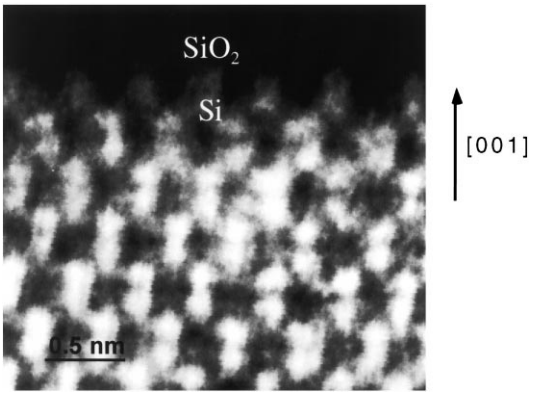

Fig. 5. Z-contrast image of a sharp Si/SiO_2 interface showing the last monolayer of Si in atomic positions close to those of the bulk.

established that significant concentrations of Ca were present in the grain boundary, approximately 0.3 monolayers, consistent with the bright intensity in the image.

To reconcile these observations with the apparently conflicting prior experimental and theoretical work, first-principles theoretical calculations were performed. These calculations in fact reproduced the results of the classical potential calculations for the clean grain boundary, indicating the open structure to be 0.5 eV lower in energy per periodic repeat unit. Theory further determined that Ca has a large segregation energy in both boundary structures, but *significantly higher* in the dense structure, sufficient to make the dense structure the lower energy boundary. These calculations therefore established that the dense structure is in fact *stabilized* by the Ca segregation, an example of a segregation-induced structural transformation [18]. Examination of the electronic charge distribution revealed just a small perturbation to the oxygen ions next to the Ca atom, indicating that the transformation is structural and not electronic in origin, i.e. it is driven by the size difference between Ca and Mg ions.

4. Structure and composition of the Si–SiO_2 interface

In the case of an amorphous material, no channeling of the probe can occur, and a Z-contrast image reflects only changes in projected atomic density. This is in marked contrast to conventional HREM images where amorphous materials always show a speckle pattern due to random interferences, and interfaces show Fresnel fringes and other coherent interference phenomena that can obscure the structure. In the Z-contrast image of Fig. 5, the last monolayer of the crystalline Si is clearly visible, and the Si columns are in almost exactly the expected positions for bulk Si [21]. Here again theory can be very useful in establishing the relative energies of various possible interface structures. Recent calculations have established that atomically abrupt interfaces are in fact energetically preferred over structures involving suboxides [22]. This is due to the softness of the Si–O–Si bond which allows strain relaxation to occur. Experimentally, however, suboxides are always found, presumably due to the non-equilibrium nature of the oxidation process and indicating the potential for improved characteristics. EELS provides a sensitive means to detect suboxides at the Si/SiO_2 interface, with high sensitivity and spatial resolution [23]. An example of an extended zone of suboxide is seen in Fig. 6, where Si-L edge spectra are plotted for a series of beam positions moving from the crystal into the oxide. The edge onset is 99 eV in the crystal, moving to 104 eV for stoichiometric SiO_2, but for approximately 2 nm both features are seen indicative of suboxide. The width of the suboxide zone is an order of magnitude greater than the beam size; this is confirmed also by profiles of the O-K edge [21], where there can be no contribution from the crystalline Si.

5. Conclusions

It is now possible to determine, without prior knowledge, the structure, impurity content and local electronic states, at grain boundaries, dislocations and interfaces by the combination of Z-contrast imaging and electron energy loss spectroscopy in the STEM. Atomic-scale total energy calculations are a natural complement and extension to these STEM techniques, giving critical insight into the underlying physics through the ability to study segregation energies, electronic states, and atomic-scale dynamics.

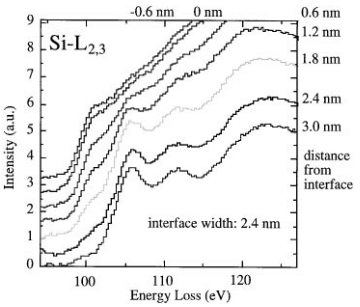

Fig. 6. Si-$L_{2,3}$ EELS profiles across a Si/SiO_2 interface showing evolution of the SiO_2 band gap. The full gap is not established until 2.4 nm into the oxide.

Acknowledgements

This research was supported by Lockheed Martin Energy Research Corp. under DOE Contract No. DE-AC05-96OR22464, ONR Grant No. N00014-95-1-0906, AFOSR Grant No. F-49620-99-1-0289 and by appointment to the ORNL Postdoctoral Research Associates Program administered jointly by ORNL and ORISE.

References

[1] L. Rayleigh, Philos. Mag. 42 (5) (1896) 167.
[2] S.J. Pennycook, in: S. Amelinckx, G. Van Tendeloo, D. Van Dyck, J. Van Landuyt (Eds.), Handbook of Microscopy, VCH Publishers, Weinheim, Germany, 1997, pp. 595–620.
[3] S.J. Pennycook, D.E. Jesson, Phys. Rev. Lett. 64 (1990) 938.
[4] S.J. Pennycook, D.E. Jesson, Ultramicroscopy 37 (1991) 14.
[5] S.J. Pennycook, D.E. Jesson, Acta. Metall. Mater. 40 (1992) S149.
[6] R.F. Loane, P. Xu, J. Silcox, Ultramicroscopy 40 (1992) 121.
[7] P.D. Nellist, S.J. Pennycook, Ultramicroscopy 78 (1999) 111.
[8] D.E. Jesson, S.J. Pennycook, Proc. Roy. Soc. A 441 (1993) 261.
[9] D.E. Jesson, S.J. Pennycook, Proc. Roy. Soc. A 449 (1995) 273.
[10] P.D. Nellist, S.J. Pennycook, Phys. Rev. Lett. 81 (1998) 4156.
[11] Y. Xin, S.J. Pennycook, N.D. Browning, P.D. Nellist, S. Sivananthan, F. Omnès, B. Beaumont, J.-P. Faurie, P. Gibart, Appl. Phys. Lett. 72 (1998) 2680.
[12] A.J. McGibbon, S.J. Pennycook, J.E. Angelo, Science 269 (1995) 519.
[13] N.D. Browning, M.F. Chisholm, S.J. Pennycook, Nature 366 (1993) 143.
[14] G. Duscher, N.D. Browning, S.J. Pennycook, Phys. Stat. Sol. A 166 (1998) 327.
[15] M.F. Chisholm, A. Maiti, S.J. Pennycook, S.T. Pantelides, Phys. Rev. Lett. 81 (1998) 132.
[16] A. Maiti, M.F. Chisholm, S.J. Pennycook, S.T. Pantelides, Phys. Rev. Lett. 77 (1996) 1306.
[17] J.R. Morris, Z.-Y. Lu, D.M. Ring, J.B. Xiang, K.M. Ho, C.Z. Wang, C.L. Fu, Phys. Rev. B 77 (1998) 11241.
[18] Y. Yan, M.F. Chisholm, G. Duscher, A. Maiti, S.J. Pennycook, S.T. Pantelides, Phys. Rev. Lett. 81 (1998) 3675.
[19] D.M. Harris, G.W. Watson, S.C. Parker, Philos. Mag. A 74 (1996) 407.
[20] W.D. Kingery, J. Am. Cer. Soc. 57 (1974) 1.
[21] G. Duscher, S.J. Pennycook, N.D. Browning, R. Rupangudi, C. Takoudis, H.-J. Gao, R. Singh, in: D.G. Seiler, A.C. Diebold, W.M. Bullis, T.J. Shaffner, R. McDonald, E.J. Walters (Eds.), Characterization and Metrology for ULSI Technology: 1998 International Conference, The American Institute of Physics, Woodbury, New York, 1998, pp. 191–195.
[22] R. Buczko, S. J. Pennycook, S. T. Pantelides, submitted for publication.
[23] D.A. Muller, T. Sorsch, S. Moccio, F.H. Baumann, K. Evans-Lutterodt, G. Timp, Nature 399 (1999) 758.